Continuum between Sorption and Precipitation of Fe(III) on Microbial Surfaces

ARTICLE *in* ENVIRONMENTAL SCIENCE AND TECHNOLOGY · JUNE 1998

Impact Factor: 5.33 · DOI: 10.1021/es9800481

2 AUTHORS:

Lesley A. Warren
McMaster University
70 PUBLICATIONS **1,451** CITATIONS
SEE PROFILE

F. Grant Ferris
University of Toronto
151 PUBLICATIONS **6,639** CITATIONS
SEE PROFILE

Environ. Sci. Technol. **1998**, *32,* 2331−2337

Continuum between Sorption and Precipitation of Fe(III) on Microbial Surfaces

LESLEY A. WARREN* AND
F. GRANT FERRIS
Department of Geology, University of Toronto, Toronto, Ontario M5S 3B1, Canada

Bacteria are a widespread, abundant, geochemically reactive component of aquatic environments. However, their role in the formation of secondary reactive surface phases such as iron oxides or in the direct sorption of metal contaminants has yet to be quantitatively described. Here, we compare the formation of iron oxides on bacterial cell surfaces to their formation abiotically (no bacteria present) over a range of both Fe(III) concentration (10^{-2}−$10^{-4.5}$ M) and pH (2−4.5) in the laboratory. Iron sorption and subsequent precipitation reactions at bacterial surfaces were modeled using current geochemical approaches. Solid-phase partitioning of Fe(III) as hydrous ferric oxide (HFO) was enhanced in the presence of a variety of bacteria over that seen in abiotic controls. The onset of HFO formation occurred at lower pH values and in greater quantities at any given pH in the bacterial treatments. Fe-(III) reactions at bacterial surfaces follow a clear continuum between sorption and precipitation that can be quantitatively described using geochemical principles and modeled using surface precipitation theory; to date only demonstrated for inorganic surfaces. These results show that the reactions at biological surfaces are likely to be important in determining the spatial distribution of iron oxides in nature and thus the reactive transport of metals in aqueous environments.

Introduction

The transport, bioavailability, toxicity, and ultimate fate of inorganic contaminants such as trace metals and radionuclides are intimately tied to the nature of reactions occurring between the contaminant and the solid phase (*1*). In recognition of the importance of reactions at solid surfaces, aquatic surface chemistry (*2*) has emerged as the conceptual framework for understanding the behavior of dissolved metals in aqueous environments through the development of surface complexation−precipitation models (SCM−SPM; *3*). These models quantify metal−solid partitioning by describing sorption and subsequent precipitation reactions between functional groups or reactive sites at the solid surface and the contaminant species and use thermodynamic equilibria as the controlling mechanism to predict when such associations are likely to occur. To date, this approach has had demonstrated success for inorganic surfaces, hydrous ferric oxide (HFO) in particular (*4*). However, a wide variety of potentially geochemically reactive substrates other than HFO occur in aquatic environments. If the SCM−SPM approach is to emerge as the guiding paradigm for metal geochemistry, its applicability to other likely important solid surfaces, e.g., both organic and inorganic, must be evaluated.

Bacteria are, at the very least, as widely distributed and probably as reactive as many inorganic solids in aquatic environments. Recognition of the role that bacteria play as geochemically reactive solids in aquatic systems stems from a large body of data demonstrating them to be both nucleation templates for a host of authigenic minerals (*5*−*7*) and potent sorbents of a wide range of dissolved metal ions (*8*−*10*). The surface reactivity of microbes arises directly from the presence of amphoteric surface functional groups (e.g., carboxyl, phosphoryl, and amino groups) that are associated with structural polymers in their cell walls and extracellular sheaths or capsules (i.e., analogous to surface hydroxyl groups on HFO). Complexation of metals by these surface functional groups is interpreted to be the mechanism underlying the sorptive properties of bacteria while the surficially sorbed metal ions are thought to furnish the sites for subsequent nucleation and precipitation of minerals (*11*−*14*).

An extensive set of experimental data exists on the interactions of metals with bacterial cells including intact whole cells, isolated cell wall fragments, and natural microbial biofilms. A common feature of these data is that metals that are prone to hydrolysis in solution appear to sorb strongly to bacterial cells. Iron(III), in particular, is known to bind tenaciously to surfaces and commonly forms insoluble HFO precipitates on bacteria in a wide range of natural environments (*15*−*17*). The surficially associated HFO creates a new surface that is highly reactive and effectively comprises a secondary sorbent phase for metal ions on the bacteria.

Recent studies suggest that metal ion interactions at bacterial cell surfaces can be described in quantitative terms using the same conceptual and mathematical approach to surface complexation that has been advanced for inorganic solids (*18*). The behavior of bacteria as heterogeneous nucleation templates for mineral precipitation also appears to conform, at least in a qualitative sense, with the basic principles of equilibrium thermodynamics, suggesting that they are amenable to quantification using geochemical modeling approaches. What has yet to be determined, however, is whether sorption and precipitation reactions at bacterial surfaces actually represent the ends of a continuum spanning surface complexation (sorption), nucleation, and precipitation as hypothesized by surface precipitation theory (*3*) and thus far demonstrated only for mineral surfaces (*19*).

If surface complexation theory can be applied to the study of geochemical reactions at bacterial surfaces, then a quantitative insight into the continuum between sorption and precipitation of dissolved metals on bacterial surfaces can be elicited. Thus far in any conceptual understanding of metal behavior in aquatic systems, the implicit assumption is that reactions should proceed homogeneously. However, reactions such as surface precipitation of secondary mineral phases on bacterial surfaces will proceed heterogeneously depending on the spatial distribution of the bacteria. To date, no quantitative understanding of the reactions at bacterial surfaces has emerged. Yet this kind of work will provide the missing link between pure chemical precipitation and the formation and synthesis of biominerals. Integration of these biological entities as another reactive substrate in developing geochemical models of aqueous contaminant behavior will vastly improve our ability to accurately predict contaminant transport, fate, and likely impacts in aquatic systems. Thus, the objectives of this study were to experi-

* Corresponding author e-mail: lwarren@zircon.geology.utoronto.ca; telephone: 416-978-0549; fax: 416-978-3938.

S0013-936X(98)00048-0 CCC: $15.00
Published on Web 06/24/1998

mentally quantify HFO formation in the presence and absence of three bacterial strains that differed in their cell surface characteristics and to demonstrate that a continuum exists between sorption and precipitation reactions of Fe(III) at these biological surfaces as anticipated from the principles of SCM−SPM.

Experimental Methods

Growth Conditions. Pure cultures of *Pseudomonas aeruginosa* H103 [Gram-negative, alginate capsule; grown in Trypticase soy broth (TSB, media pH ~7)], *Bacillus subtilis* [Gram-positive, no capsule; grown in brain heart infusion (BHL media pH ~7)], and *Bacillus licheniformis* (Gram-positive, polyglutamic acid capsule; grown in BHL) were obtained for experimental assays by incubating overnight at 37 °C. For all three bacterial strains, cells for use in subsequent Fe experiments were obtained by rinsing twice with ultrapure water and resuspension in ultrapure water (cell resuspension pH ~ 7). Cell densities used in the experiments were equivalent to an optical density of 0.2 at 600 nm (~10^8 cells/mL, DAPI counts on cell resuspensions in ultrapure water). Optical densities were measured spectrophotometrically at 600 nm using a Milton Roy Spectronic 1001 Plus. While we cannot comment on cell viability throughout the experiments, visual inspection of cells at the end of experiments indicated that they remained intact throughout the experimental manipulation, i.e., no lysis occurred.

Iron Partitioning Experiments. Iron partitioning (dissolved−solid phases) experiments were carried out over a range of both Fe(III) concentration [10^{-2}−$10^{-4.5}$ M at $10^{-0.5}$ M increments; Fe(III) added as $Fe(NO_3)_3{\cdot}6H_2O$] and pH (2−4.5 at 0.5 pH increments; pH was monitored and maintained at ±0.1 pH unit of the nominal pH value during each experimental run) under nongrowth conditions [cell concentrations equivalent to an optical density of 0.2 (600 nm)] in laboratory assays (2 h exposure at room temperature, gently shaken, maintained at constant pH, and run at low ionic strength (the highest ionic strength of any of the experimental treatments ≤ 0.005 for $Fe_T = 0.01$M)]. In the modeling of the data, concentrations were assumed equal to activity. These experiments were carried out for each of the three bacterial strains as well as for an abiotic control treatment (no bacteria present). In all experiments, particulate Fe concentrations (Fe_S) were determined by difference between total Fe (Fe_T) and dissolved Fe (Fe_D; 0.2 μm filtered using sterile acrodisc filters with Supor membrane) using a phenanthroline spectrophotometric assay.

Transmission Electron Microscopy and Energy Dispersive X-ray Spectroscopy (TEM/EDS). In addition to analyses of Fe_T and Fe_D concentrations, the association of Fe at the bacterial surfaces was determined by direct examination of the bacterial surfaces using transmission electron microscopy (TEM) and energy-dispersive X-ray spectroscopy (EDS) analyses. For the TEM/EDS analyses, 1-mL subsamples from the bacterial treatment Fe partitioning experiments were centrifuged for 2 min, and the pellets were then rinsed twice with ultrapure water and resuspended in 50 μL of ultrapure water. Samples were then directly deposited on carbon coated nickel or copper grids with supporting Formvar film. Elemental analyses of whole mounts were immediately obtained using a Philips EM400T electron microscope equipped with an X-ray spectrometer [Link Analytical eXL/LZ-5; EDS performed at 100 kV with a beam current of 10 nA for 100 seconds (live time)].

Results and Discussion

Solid-Phase Partitioning of Fe(III). For a given pH, Fe_S concentrations in all three bacterial addition treatments were higher than those observed in the chemical controls (no bacteria present) confirming that the presence of bacteria enhances solid-phase partitioning of iron (Figure 1). In the control treatment, the formation of particulate Fe only occurred at pH values above 3 at an Fe_T of 10^{-4} M and at pH values above 2 in $Fe_T = 0.01$ M, indicating a high degree of supersaturation for amorphous iron oxides (Figure 1). In contrast, enhanced solid-phase partitioning of Fe(III) was observed in the bacterial treatments, spanning a range of pH values below the equilibrium solubility of poorly ordered HFO precipitates [i.e., <3 for $Fe_T = 10^{-4}$ M and $\log K_{s0} = 5.0$ (*20*); Figure 1], implying that either sorption had occurred or that crystalline HFOs had precipitated. Fe_S concentrations in the control treatment were lower than those predicted by equilibrium speciation calculations (Mineql, V 3.0), which probably reflects a lack of true equilibrium due to the relatively short 2-h experimental period. Thus, the results should be interpreted to indicate bacterial enhancement of the rate of formation of HFO rather than increased HFO formation.

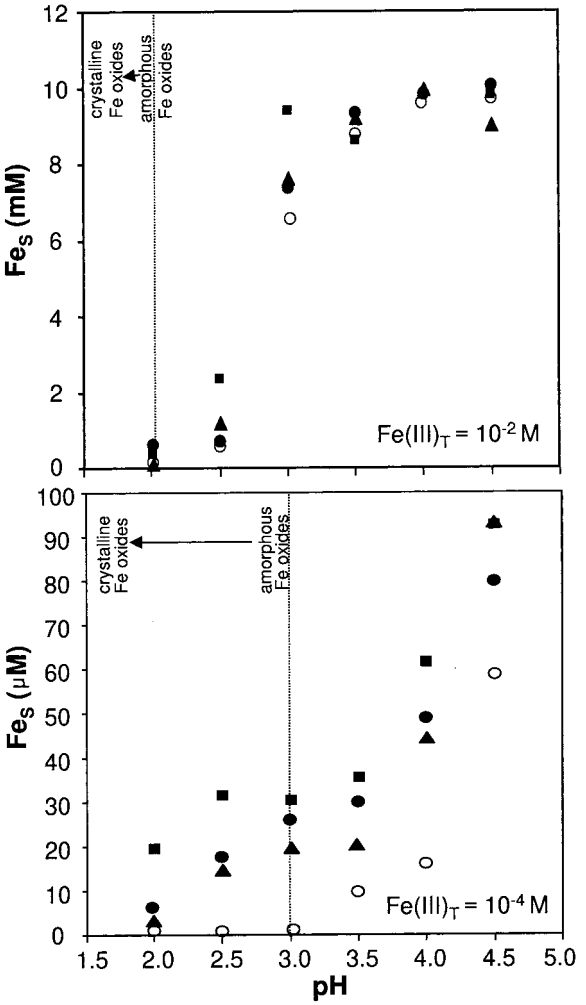

FIGURE 1. Particulate iron (Fe_S) as a function of a pH gradient (2−4.5 at 0.5 unit increments) in control (○) and bacterial addition treatments (*B. subtilis* ■, *B. licheniformis* ●, *P. aeruginosa* ▲) for total iron Fe_T concentrations of 10^{-4} and 10^{-2}M (note differences in *y* axis scales). These results are shown as representative of the entire concentration gradient examined (10^{-2}−$10^{-4.5}$ M Fe_T at 0.5 M increments). The dashed vertical lines indicate the pH at which supersaturation with respect to amorphous FeOOH(s) occurs, and the arrow indicates the pH range over which a variety of HFOs might form from more crystalline (i.e., goethite) at lower pH values to more amorphous HFOs such as ferrihydrite (pH 3 at $Fe_T = 10^{-4}$ M; pH = 2 at $Fe_T = 10^{-2}$ M) at higher pH values (*20*, *23*).

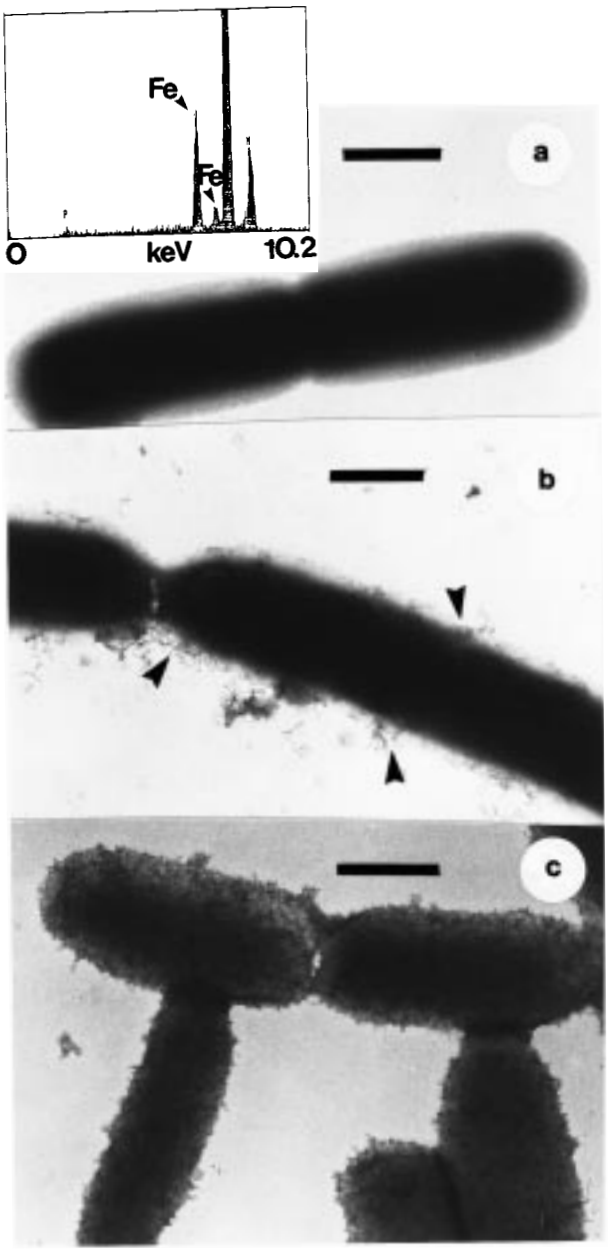

FIGURE 2. TEM and associated EDS spectra for *P. aeruginosa* exposed to 10^{-4} M Fe at pH 2 (a), 3 (b), and 4 (c). At pH 2 (a), the bacterial cells show no Fe precipitates; however, the EDS spectra confirms the presence of Fe on the cell surface consistent with sorption mechanisms. At pH 3 (b), Fe precipitates are clearly visible in the TEM pictures (noted by arrows); while at pH 4 (c), the cell surfaces are completely coated with Fe precipitates. Scale, bars = 500 nm.

TEM examination and EDS analyses confirmed that solid-phase partitioning of Fe(III) occurred directly on the bacterial cell surfaces (Figure 2). At low Fe_T, no HFO precipitates developed away from the cells (i.e., through homogeneous precipitation in solution). Bulk extracellular HFO precipitation was only observed at high pH and high Fe_T (10^{-2} M) values where bacterial cell and control Fe_S data converged (see Figure 1). At the lowest pH examined (pH = 2), no visible precipitates were evident on the cell surface (Figure 2a); however, corresponding EDS spectra for the bacteria clearly revealed Fe consistent with the presence of sorbed Fe(III). At the higher pH values (Figure 2b,c), distinct fine-grained Fe precipitates, 10−20 nm in diameter, were evident on cell surfaces indicating that HFO formation had occurred as pH increased and that the cells had participated as heterogeneous nucleation templates for HFO precipitation. Selected area electron diffraction analyses of the precipitates revealed diffuse reflections around $d = 0.15$ and 0.26 nm, indicating that the HFO precipitates were poorly ordered ferrihydrite not more crystalline HFO as might have been supposed from the results presented in Figure 1. These results indicate that the presence of the bacteria initiated the formation of ferrihydrite at a lower degree of supersaturation compared to the chemical controls.

Fe(III) Surface Reactions. The continuum between cation sorption and precipitation reactions at mineral surfaces has been demonstrated to represent an evolution of surface reactions through three distinct stages. The initial sorption stage (two-dimensional association with the surface) is followed by surface site saturation, and once critical supersaturation has been reached, precipitation (three-dimensional configuration; *2*, *20*). If such a continuum of Fe reactions occurs at bacterial surfaces, then all three stages should be evident in isotherms relating the solid-phase concentration of Fe(III) to the equilibrium proton condition and the concentration of Fe(III) remaining in solution. This relationship is inferred from the overall reaction for Fe(III) sorption and hydrolysis on bacteria that incorporates the ion concentration ratio $[Fe^{3+}]/[H^+]^3$ defining solubility equilibria for HFO (K_{SO}):

$$BH + Fe^{3+} + 2H_2O \rightleftarrows BFe(OH)_2^0 + 3H^+ \qquad (1)$$

where BH represents a bacterial surface site (analogous to ≡SOH for iron oxides) and $BFe(OH)_2^0$ is bacterially associated Fe. The corresponding apparent surface complex formation constant, K^s_{Fe} is given by

$$K^s_{Fe} = \frac{[BFe(OH)_2^0][H^+]^3}{[BH][Fe^{3+}]} \qquad (2)$$

where $BFe(OH)_2^0$ can be estimated by Fe_S and Fe^{3+} can be estimated by Fe_D. This expression implicitly embodies a set of mass action relationships that describe the hydrolysis of Fe(III) in solution, sorption of individual Fe(III) hydrolysis species, and formation of Fe(III) surface hydroxo complexes.

In double logarithmic plots of experimental equilibrium data (Figure 3), the linear portion of the curves at low $[Fe_D]/[H^+]^3$ values indicate that sorption was directly proportional to $[Fe_D]/[H^+]^3$ with slopes close to unity. This type of fit is indicative of Langmuir behavior and implies that the sorptive affinity of Fe(III) for the bacterial surface remains fairly constant until site saturation is approached (*20*). The second stage of surface site saturation and onset of supersaturation is evidenced where the curves plateau as $[Fe_D]/[H^+]^3$ values increase. The third stage of precipitation is marked by a sharp increase in solid-phase Fe concentrations, typically at $[Fe_D]/[H^+]^3$ values that exceed the recognized equilibrium solubility of poorly ordered HFO and indicates that stable critical nuclei necessary for the onset of surface precipitation have formed. The curves then undergo a reversal as the ion concentration ratio decreases, and HFO precipitation becomes the dominant process contributing to the solid-phase partitioning of Fe(III).

Combining the mass action relationship for the sorption and hydrolysis of Fe(III) on bacteria with the corresponding mass balance expression for total reactive surface sites on cells provides a more formal Langmuir sorption equation:

$$[BFe(OH)_2^0] = ([B_{max}]K^S_{Fe}([Fe_D]/[H^+]^3))/(1 + K^S_{Fe}([Fe_D]/[H^+]^3)) \qquad (3)$$

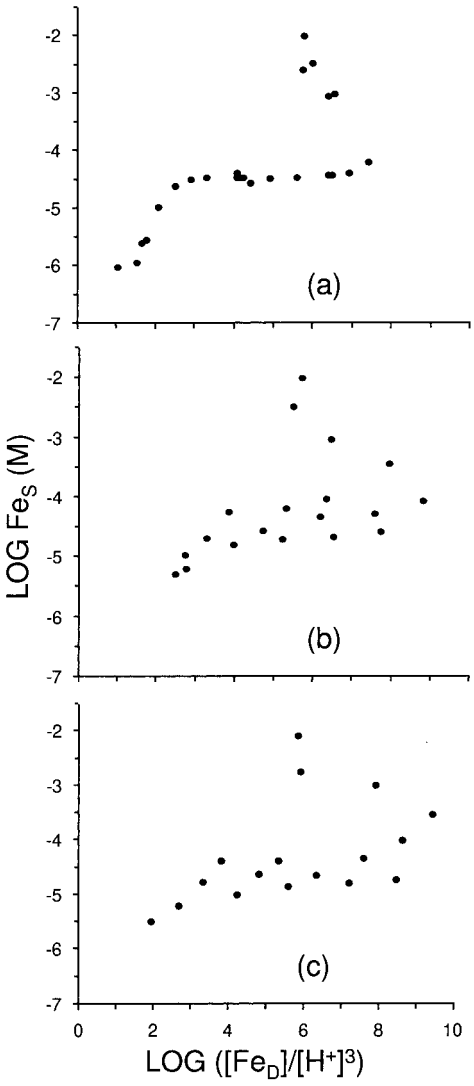

FIGURE 3. Log Fe_S (M) as a function of log($[Fe_D]/[H^+]^3$) for the three bacterial strains examined: *B. subtilis* (a), *B. licheniformis* (b), and *P. aeruginosa* (c). The data points are from the series of experiments in which both Fe_T and pH were varied. The modeling of Fe sorption, nucleation, and precipitation to these microbial surfaces is achieved with a simple mass action expression that uses a generalized bacterial surface site (eq 1). Data are more variable for the two encapsulated species (*B. licheniformis* and *P. aeruginosa*), probably due to some breakage of the capsules during analyses. Results indicate that Fe reactions with live biological surfaces follow Langmuir-type isotherm behavior. Double-reciprocal plots of the sorptive part of the curve yield log K^S_{Fe} and maximum binding capacity values (see Table 1).

where B_{max} is the total Fe(III) binding capacity of the bacteria and $[B_{max}] = [BH] + [BFe(OH)_2^0]$.

In a reciprocal form, the Langmuir equation permitted calculation of apparent surface complex formation constants (K^S_{Fe}) and maximum binding capacities from the experimental sorption data obtained with each of the three bacteria examined in the study (Table 1). Selection of data points for the double-reciprocal plots was based on the linear portion of the curve at low log($[Fe_D]/[H^+]^3$) values as well as those points at the onset of the plateau phase that were within the confidence intervals for the slope of the linear regression. Regression analysis of the double-reciprocal plots established that over 88−97% of the variance in the sorption data can be attributed directly to the equilibrium $[Fe(III)]/[H^+]^3$ concentration ratio. These strong correlations emphasize the utility of applying the basic principles of surface complexation theory to chemically and structurally heterogeneous particulate solids such as bacterial cells, as has been suggested by Sigg (*21*).

The K^S_{Fe} values ranged from approximately $10^{-2.5}$ for *B. subtilis* and *P. aeruginosa* to $10^{-3.5}$ for *B. licheniformis* (Table 1). We have only been able to find one other surface complex formation constant for Fe(III) sorption to solid surfaces (*22*). Specifically a K^S_{Fe} of $10^{-1.77}$ was reported by Schindler et al. (*22*) for sorption of Fe onto silica which, while somewhat higher, still agrees favorably with our values.

The correlation between the first hydrolysis constant in solution and uptake on a solid surface reflects the affinity of the metal for the solid surface hydroxyl groups; thus, the larger the hydrolysis constant, the larger the surface formation complex constant is likely to be (*23*). This relationship has been specifically demonstrated for cations sorbing to HFOs (*4*). The correlations between our Fe surface formation complex constants determined for bacterial surfaces as well as the Fe surface formation complex constant determined for silica by ref *22* and the first hydrolysis constant for Fe conform well with the cation−HFO relationship reported by Dzombak and Morel (*4*; Figure 4). The regression equation determined by ref *4* remains highly significant with inclusion of the Fe points while neither the slope or intercept values are significantly affected by inclusion of our data. This result has two important implications: one, the correlation between the ability of metals to hydrolyze and their affinity for surfaces is applicable to more than just HFO surfaces; and two, sorptive reactions at bacterial surfaces that probably involve different surface functional groups such as carboxyl and phosphoryl groups are similar to those that occur at mineral surfaces such as HFOs and silica involving hydroxyl surface groups, i.e., the correlation appears to hold irrespective of the functional group involved.

The differences observed in K^S_{Fe} among the three bacteria probably reflect subtle variations in the chemical composition and structural configuration of surface sorption sites on the cells. Notably, the extracellular polyglutamic acid capsule of *B. licheniformis* is composed of an amino acid, while the Gram-positive cell wall of acapsular *B. subtilis* and alginate capsule of *P. aeruginosa* are comprised of highly modified polysaccharides (*24*, *25*).

On a molar basis, the maximum sorptive capacities of the bacteria (at equivalent suspension densities of $o.d._{600} = 0.2$) fall within the same order of magnitude and approach the millimole per gram range when normalized by cell dry weight (Table 1). Of the three bacteria, *B. licheniformis* exhibited the highest sorptive capacity, followed by *B. subtilis*, and then *P. aeruginosa*. This trend is consistent with previous work, which has shown that Gram-positive bacteria, particularly encapsulated species, are capable of binding more metal than their Gram-negative counterparts (*26*). The reason for this is the higher density of amphoteric groups in the walls of Gram-positive bacteria relative to the outer membrane of Gram-negative bacteria.

Fe(III) Precipitation on Bacterial Surfaces. In the transition from sorption to surface precipitation, equilibrium $[Fe_D]/[H^+]^3$ ratios increased beyond the solubility limits reported for fresh HFO precipitates (Figures 1 and 3; *20*). This trend of apparent oversaturation in the experimental data can be explained by the progressive formation and dissolution of unstable polynuclear Fe(III) surface hydroxo complexes on the bacterial cells. Typically, the formation of simple mononuclear Fe(III) hydrolysis species is very fast, while polynuclear hydroxo complexes that are kinetic intermediates in the transition of free Fe(III) ions to solid precipitates often form rather slowly. The differing kinetic rates of formation tend to give rise to metastable supersaturation, a condition that reflects both the slow transition of polynuclear hydroxo complexes into solid precipitates and

TABLE 1. Apparent Surface Complex Formation Constants (K^s_{Fe}) and Maximum Binding Capacities (BFe_{max}) Determined for the Three Microbial Taxa (Values Calculated from Double-Reciprocal Plots Using the Linear Portion of the Curve from Figure 3)

treatment	n^a	$r^{2\,b}$	log K^s_{Fe}	log BFe_{max} (M)	log $BFe_{max}{}^c$ (mol g^{-1} cells^{-1})
B. subtilis	8	0.97	−2.4	−4.7	−3.1
B. licheniformis	5	0.88	−3.5	−4.3	−2.9
P. aeruginosa	4	0.91	−2.6	−4.8	−3.6

[a] Where *n* equals the data points used for the double-reciprocal plots (selection of data points for the double-reciprocal plots was based on the linear portion of the curve at low log($[Fe_D]/[H^+]^3$) values as well as those data points at the onset of the plateau phase that were within the confidence intervals for the slope of the linear regression (the values were not significantly different by omitting these data points; *2*). [b] All regressions were statistically significant at the $p < 0.01$ level (Statistica V. 4.5). [c] Equivalent dry weights were determined for each strain for an optical density of 0.2.

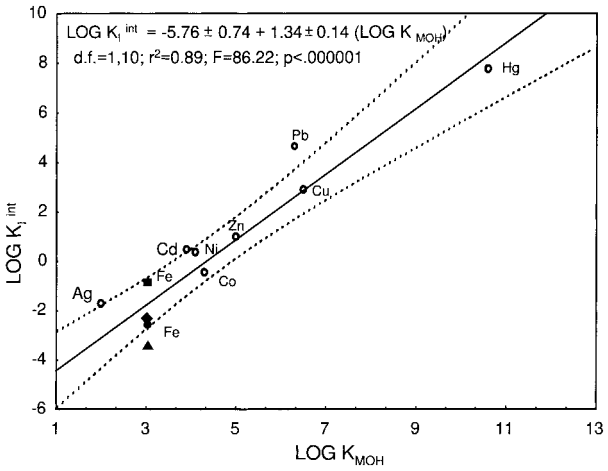

FIGURE 4. Log K_i^{int} (using terminology from ref *4*; log K^S_{Fe} in this study) versus the first hydrolysis constant (log K_{MOH}) using data reported by ref 4 for cation surface complex formation on HFO and including our surface complex constants for Fe sorption to bacterial surfaces (*B. subtilis* ♦, *B. licheniformis* ●, *P. aeruginosa* ▲) and the value for Fe sorption to silica from Schindler et al. (*22*; ■). The dotted lines indicate the 95% confidence interval for the slope.

the higher solubility associated with extremely fine-grained fresh HFO precipitates (*20*). Eventually, however, stable critical nuclei formed on the bacteria that supported and sustained crystal growth. The subsequent transformation of the initial Fe(III) surface complexes into HFO crystallites recognizable by TEM was accompanied by a decrease in the equilibrium $[Fe(III)]/[H^+]^3$ ratio with increasing amounts of solid-phase Fe(III) (Figure 3).

The solubility of fine-grained precipitates is described quantitatively by (*2*, *20*)

$$\mathrm{d}\ln K_{s0}/\mathrm{d}S = 2/3\,\gamma/RT \tag{4}$$

or

$$\log K_{s0(S)} = \log K_{s0(S=0)} + (2/3\gamma/2.3RT)S \tag{5}$$

where γ is the mean free surface energy or interfacial tension (J m^{-2}) and S is the molar surface (m^2 mol^{-1}). The molar surface can be expressed by

$$S = (s/v)(Fe_P{}^{-1}) \tag{6}$$

where s/v represents the surface area to volume ratio of the stable critical nucleus required for precipitation (in m^2 L^{-1}) and Fe_P is the concentration of precipitated Fe(III) (in mol L^{-1}). If it is assumed that all solid-phase Fe above values of BFe_{max} is precipitated iron, then Fe_P can be calculated by subtracting BFe_{max} from all values of BFe_S that exceed BFe_{max}. By also considering the solubility of $Fe(OH)_3$:

$$Fe(OH)_3 + 3H^+ \rightleftarrows Fe^{3+} + 3H_2O \qquad K_{s0} = \frac{[Fe^{3+}]}{[H^+]^3} \tag{7}$$

and substituting for S from eq 6 and for k_{s0} from eq 7 into eq 5 leads to:

$$\log [Fe_D]/[H^+]^3 = \log K_{s0(S=0)} + (2/3\gamma/2.3RT)(s/v)(Fe_P{}^{-1}) \tag{8}$$

A plot of log $[Fe_D]/[H^+]^3$ versus $Fe_P{}^{-1}$ thus yields a slope of $(2/3\gamma/2.3RT)$ (s/v) from which the surface area to volume ratio (m^2 L^{-1}) of the precipitating nuclei can be determined and an intercept of log $K_{s0(S=0)}$ (Table 2; Figure 5). Inspection of these results shows that the limiting solubility constants agree well, both among bacterial treatments and between bacterial and control treatments. However, the slopes of the bacterial relationships are lower than that of the chemical control, indicating that the bacteria enhance the thermodynamic stability and transformation of nascent critical nuclei into solid HFO precipitates. The experimental log K_{s0} values are consistent with solubility products reported in the literature for fresh, fine-grained, HFO precipitates (*23*).

Assuming an interfacial surface tension for HFO of 1.6 J m^{-2} (*2*), the s/v ratio of the nascent precipitates under abiotic conditions is on the order of 1.8 m^2 L^{-1} (Table 2). The s/v ratios calculated for the bacteria are considerably lower, ranging from 0.2 to 0.9 m^2 L^{-1}. Since TEM revealed a fairly uniform size distribution of HFO precipitates in the various experiments, these differences can only be explained by the formation of a new interface in response to heterogeneous nucleation and surface precipitation on the bacteria, i.e., while the total HFO surface area remains constant, direct contact between the precipitates and bacteria cell surface leaves a reduced area exposed to solution. Further calcula-

TABLE 2. Calculated Values of Nucleation and Precipitation Parameters for HFO Formation on the Three Strains of Bacteria Examined and in the Chemical Control Treatments (see Figure 5)

treatment	n	$r^{2\,a}$	s/v^b (m^2 L^{-1})	s^c (m^2 g^{-1})	$\Delta G_i{}^d$ (KJ mol^{-1})
controls	6	0.75	1.8	468	54
B. subtilis	6	0.95	0.9	227	26
B. licheniformis	5	0.95	0.2	55	6
P. aeruginosa	4	0.70	0.5	120	14

[a] All statistical analyses significant at the $p < 0.05$ level (Statistica V 4.5). [b] Calculation of s/v value was achieved using the slopes determined for eq 2, using a value of γ equal to 1.6 J m^{-2} (goethite; *2*). [c] s or surface area exposed in m^2 g^{-1} can be estimated by dividing s/v values by the density of the solid phase. In this case, we assumed the HFO to be equivalent to $Fe(OH)_3$, with a density of 3.96 mg L^{-1} (*23*). [d] ΔG_i values can be estimated by multiplying s by the HFO formula weight and $2/3\gamma$ (assuming a γ of 1.6 J m^{-2}; *2*).

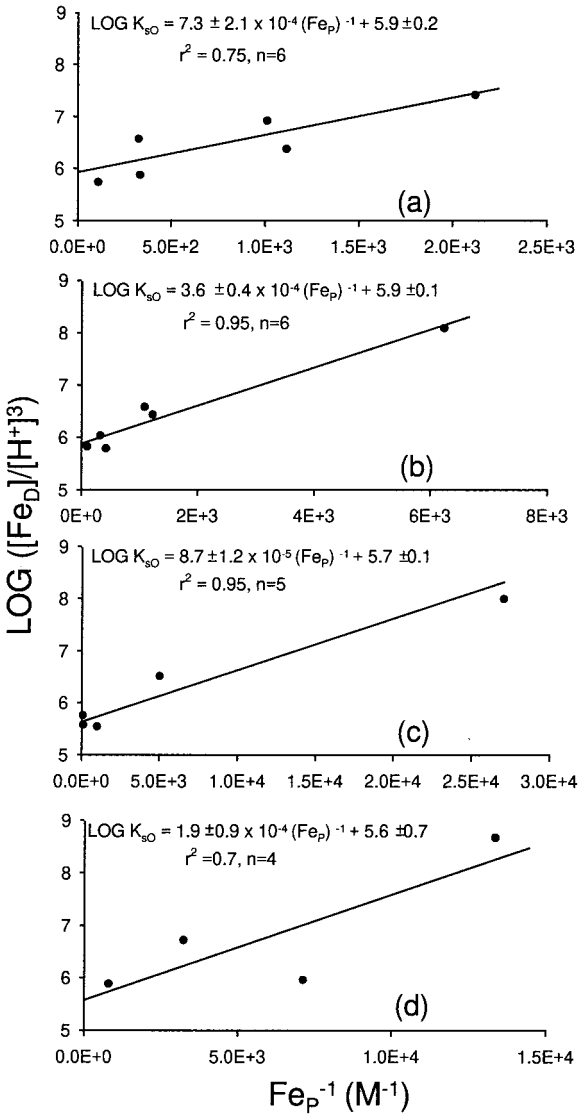

FIGURE 5. Log ([Fe_D]/[H^+]^3) versus 1/Fe_P (M^{-1}) for the chemical controls (a) and the three microbial taxa: *B. subtilis* (b), *B. licheniformis* (c), and *P. aeruginosa* (d; see eq 8). The relationships are statistically significant at the $p < 0.05$ level (Statistica version 4.5). The intercepts of all four relationships, representing log K_{s0} (s=0) for the nucleating HFO are similar, suggesting an initial value around 5.8.

tion (see Table 2) leads to a specific surface area for the precipitates of 468 $m^2\ g^{-1}$ in the chemical controls, within range of the commonly used value for HFO surface area of 600 $m^2\ g^{-1}$ (*4*). Conversely, the exposed surface area for the bacterial precipitates ranges from 227 $m^2\ g^{-1}$ for acapsular *B. subtilis* to 55 and 120 $m^2\ g^{-1}$ for encapsulated *B. licheniformis* and *P. aeruginosa*, respectively. The low HFO surface area for the two encapsulated bacteria implies that the precipitates developed directly within a matrix of extracellular polymeric material, as is often observed in natural microbial biofilms (*8*−*10*, *15*−*17*).

The interfacial free energies [ΔG_i, the energy that has to be overcome between the nascent crystal nucleus and either the solution (homogeneous nucleation) or solid surface (homogeneous nucleation) for nucleation to occur; 2] of the precipitates, estimated from HFO surface areas, were substantially reduced in response to surface precipitation on the bacterial cells (Table 2). The 2−10-fold decrease in ΔG_i values indicates clearly that thermodynamic activation energy barrier constraints on HFO formation are abated through bacterial cell surface nucleation and precipitation. Again, the encapsulated bacteria display the lowest ΔG_i values.

Our results provide the first demonstration of the continuum among sorption, nucleation, and precipitation of HFOs on microbial cell surfaces and allowed quantification of the ability of microbes to enhance HFO formation. We speculate that our results using ordinary heterotrophic bacteria in the laboratory may be analogous to metabolically mediated HFO production in nature, by Fe(II) oxidizing bacteria. The biologically produced Fe(III) could potentially sorb to the bacterial surface and ultimately precipitate according to the same principles we have demonstrated with heterotrophic bacteria under nongrowth conditions. Furthermore, we presume that HFO precipitates on bacteria have similar sorptive capacities for metals and radionuclides as abiotically produced HFOs. Overall, these results have important consequences for aqueous geochemical modeling, especially in subsurface environments where microbially controlled reactions often play a key role in determining the fate and transport of contaminants. An important implication of this work is that physical and environmental factors regulating the spatial distribution and abundance of microorganisms are apt to profoundly influence the deposition of HFO and thus the chemical reactivity of aquatic systems. The concept of microbial control on the rates and locations of geochemical reactions (e.g., sorption, precipitation) has thus far been largely ignored in any paradigm development for reactive transport in natural systems.

Acknowledgments

We thank Danielle Fortin for preparation of microbial cultures and technical assistance and G. Anderson, A. Tessier, J. Zachara, and three anonymous reviewers for constructive comments. L.W. was supported by the U.S. Department of Energy, Office of Health and Environmental Research, through the Subsurface Program.

Literature Cited

(1) Stumm, W.; Sigg, L.; Sulzberger B. In *Chemical and Biological Regulation of Aquatic Systems;* Buffle, J., DeVitre, R., Eds.; Lewis: Boca Raton, 1994; Chapter 2.
(2) Stumm, W. *Chemistry of the Solid-Water Interface;* Wiley-Interscience: New York, 1992.
(3) Farley, K. J.; Dzombak, D. A.; Morel, F. M. M. *J. Colloid Interface Sci.* **1985**, *106*, 226.
(4) Dzombak, D. A.; Morel, F. M. M. *Surface Complexation Modelling: Hydrous Ferric Oxide;* Wiley-Interscience: New York, 1990.
(5) Ferris, F. G.; Beveridge, T. J.; Fyfe, W. S. *Nature* **1986**, *320*, 609.
(6) Ferris, F. G.; Fyfe, W. S.; Beveridge, T. J. *Chem. Geol.* **1987**, *63*, *225*.
(7) Ferris, F. G.; Fratton, C. M.; Gerits, J. P.; Schultze-Lam, S.; Sherwood-Lollar, B. *Geomicrobiol. J.* **1995**, *13*, *57*.
(8) Beveridge, T. J. *Annu. Rev. Microbiol.* **1989**, *43*, 147.
(9) Ferris, F. G. *Earth Sci.* **1993**, *47*, *233*.
(10) Schultze-Lam, S.; Thompson, J. B.; Beveridge, T. J. *Water Pollut. Res. J. Can.* **1993**, *28*, 51.
(11) Kurek, E.; Czaban, J.; Bollag, J. M. *Appl. Environ. Microbiol.* **1982**, *43*, 1011.
(12) Beveridge, T. J.; Meloche, J. D.; Fyfe, W. S.; Murray, P. G. E. *Appl. Environ. Microbiol.* **1983**, *45*, 1094.
(13) Walker, S. G.; Fleming, C. A.; Ferris, F. G.; Beveridge, T. J.; Bailey, G. W. *Appl. Environ. Microbiol.* **1989**, *55*, 2976−2984.
(14) McLean, R. J. C.; Fortin, D.; Brown, D. A. *Can. J. Microbiol.* **1996**, *42*, 392−400.
(15) Ferris, F. G.; Schultze, S.; Witten, T. C.; Fyfe, W. S.; Beveridge, T. J. *Appl. Environ. Microbiol.* **1989**, *55*, 1249.
(16) Mann H.; Fyfe, W. S. *Can. J. Earth Sci.* **1989**, *26*, 2731.
(17) Konhauser, K. O.; Ferris, F. G. *Geology*, **1996**, *24*, 323.
(18) Fein, J. B.; Daughney, C. J.; Yee, N.; Davis, T. A. *Geochim. Cosmochim. Acta* **1997**, *61*, 3319.

(19) Comans, R. N. J.; Middelburg, J. J. *Geochim. Cosmochim. Acta* **1987**, *51*, 2587.
(20) Stumm, W.; Morgan, J. J. *Aquatic Chemistry*, 3rd ed.; Wiley-Interscience: New York, 1996.
(21) Sigg, L. In *Chemistry of the Solid-Water Interface*; Stumm, W., Ed.; Wiley-Interscience: New York, 1992; Chapter 11.
(22) Schindler, P. W.; Fürst, B.; Dick, R.; Wolf, P. U. *J. Colloid Interface Sci.* **1976**, *55*, 469.
(23) Cornell, R. M.; Schwertmann, U. *The Iron Oxides*; VCH: New York, 1996.
(24) Ferris, F. G.; Beveridge, T. J. *Bioscience* **1985**, *35*, 172.
(25) Beveridge, T. J. In *Bacteria in Nature*, Vol. 3; Poindexter, J. S.; Leadbetter, E. R., Eds.; Plenum: New York, 1989; Chapter 1.
(26) Mullen, M. D.; Wolf, D. C.; Ferris, F. G.; Beveridge, T. J.; Flemming, C.; Bailey, G. W. *Appl. Environ. Microbiol.* **1989**, *55*, 3143.

Received for review January 21, 1998. Revised manuscript received May 15, 1998. Accepted May 15, 1998.

ES9800481